Article

Microstructure and Hydrogen Permeability of Nb-Ni-Ti-Zr-Co High Entropy Alloys

Egor Kashkarov [1],[*] , Dmitriy Krotkevich [1] , Maxim Koptsev [1], Sergei Ognev [1], Leonid Svyatkin [1] , Nahum Travitzky [1,2] and Andrey Lider [1]

[1] School of Nuclear Science and Engineering, National Research Tomsk Polytechnic University, 634050 Tomsk, Russia

[2] Department of Materials Science, Glass and Ceramics, Friedrich-Alexander-Universität Erlangen-Nürnberg, 91054 Erlangen, Germany

[*] Correspondence: ebk@tpu.ru; Tel.: +7-3822-70-17-77 (ext. 1562)

Abstract: Hydrogen separation membranes are one of the most promising technologies for hydrogen purification. The development of high-entropy alloys (HEAs) for hydrogen separation membranes is driven by a "cocktail effect" of elements with different hydrogen affinities to prevent hydride formation and retain high permeability due to the single-phase BCC structure. In this paper, equimolar and non-equimolar Nb-Ni-Ti-Zr-Co high entropy alloys were fabricated by arc melting. The microstructure and phase composition of the alloys were analyzed by scanning electron microscopy and X-ray diffraction, respectively. The hydrogen permeation experiments were performed at 300–500 °C and a hydrogen pressure of 4 bar. In order to estimate the effect of composition and lattice structure on hydrogen location and diffusivity in Nb-Ni-Ti-Zr-Co alloy, ab initio calculations of hydrogen binding energy were performed using virtual crystal approximation. It was found that Nb-enriched and near equimolar BCC phases were formed in $Nb_{20}Ni_{20}Ti_{20}Zr_{20}Co_{20}$ HEA while Nb-enriched BCC and B2-Ni(Ti, Zr) were formed in $Nb_{40}Ni_{25}Ti_{18}Zr_{12}Co_5$ alloy. Hydrogen permeability tests showed that $Nb_{20}Ni_{20}Ti_{20}Zr_{20}Co_{20}$ HEA shows lower activation energy and higher permeability at lower temperatures as well as higher resistance to hydrogen embrittlement compared to $Nb_{40}Ni_{25}Ti_{18}Zr_{12}Co_5$ alloy. The effect of composition, microstructure and hydrogen binding energies on permeability of the fabricated alloys was discussed.

Keywords: high-entropy alloys; membranes; microstructure; ab initio calculation; hydrogen permeability

1. Introduction

Membrane technology is one of the most efficient approaches for hydrogen separation and purification due to low operating costs, high productivity and low power consumption [1,2]. Metal membranes have the highest selectivity for hydrogen separation. Thin Pd foils have a separation factor >1000 [1]. Palladium-based (Pd-based) membranes with a face centered cubic (fcc) lattice structure have the ability to dissociate and dissolve molecular hydrogen and thus exhibit excellent H_2 permeability properties [3]. However, the high cost of Pd motivates researchers to develop composite membranes or alternative effective membrane materials [4].

The V metals group (V, Nb, Ta, etc.), with a more open body-centered cubic (BCC) lattice, are more permeable to hydrogen and are promising candidate materials for hydrogen separation membranes [5,6]. However, in most cases the single-element membranes of the V group suffer from hydrogen embrittlement (HE) and gas poisoning at high temperature, which does not allow their wide use for hydrogen separation in industry [7]. Thus, multicomponent alloys based on V group elements with a BCC structure, which are more resistant to embrittlement, are being developed [8,9]. It is well known that the composition of alloys significantly affects its hydrogen permeability and resistance to HE [10].

It was shown that alloying of Nb-based alloys with Ti and Ni can lead to a reduction of hydrogen embrittlement and permeability [11,12]. In addition to the formation of BCC phases, interdendritic TiNi compounds inhibit hydride formation. Ni stabilizes the alloy with reduced H absorption. The presence of Ti in Nb-based alloys increases the thermal stability and hydrogen absorption [9,13]. The addition of Zr in Ni-Nb-Zr-Co alloy increases hydrogen sorption and increases permeability; however, it reduces the resistance to HE. The addition of Co is effective in suppressing hydrogen embrittlement of Ni-Nb-Zr-Co alloy [14]. Tang et al. investigated multicomponent $Nb_{40}Ti_{18}Zr_{12}Ni_{25}M_5$ (M = Al, Co, Cu, Pd) and showed that the $Nb_{40}Ti_{18}Zr_{12}Ni_{25}Co_5$ alloy had the highest permeability of 3.8×10^{-8} ($molH_2m^{-1}s^{-1}Pa^{-0.5}$), higher than that for $Pd_{0.23}Ag_{0.77}$ alloy, with a permeability of 1.6×10^{-8} ($molH_2m^{-1}s^{-1}Pa^{-0.5}$), while maintaining stable performance [15].

Multicomponent alloys with more than four elements in near equimolar composition, also known as high-entropy alloys (HEAs), can be considered as membrane materials. The "cocktail effect" [16] of elements with different hydrogen affinities can provide low hydrogen embrittlement and high permeability due to the single phase BCC crystal structure. It was reported that high-entropy alloys have high mechanical strength, which is maintained over a wide temperature range, phase stability and low degradation rate [17]. Han et al. demonstrated high phase stability and mechanical properties for $Nb_{20}Ni_{20}Ti_{20}Co_{20}Zr_{20}$ under compressive tests up to 800 °C [18]. However, there are no experimental works on the hydrogen permeability of this HEA. Therefore, in the present work, based on the positive effect of alloying elements we selected the Nb-Ni-Ti-Zr-Co system to fabricate equimolar and non-equimolar high-entropy alloys and investigated its microstructure and hydrogen permeability.

2. Materials and Methods

2.1. Material Preparation

Metal powders of Nb, Ni, Ti, Zr, Co (>99.5% purity) were mixed in a ball mill (AGO-2: Novits, Novosibirsk, Russia) to obtain homogeneous distribution of elemental powders. The powders were mixed with the rotation speed of 170 rpm for 1 h. Two series of powders with equimolar composition ($Nb_{20}Ni_{20}Ti_{20}Zr_{20}Co_{20}$) and non-equimolar composition ($Nb_{40}Ni_{25}Ti_{18}Zr_{12}Co_5$) were prepared. The mixed powders were pressed by a cold static uniaxial method at the pressure of 90 MPa in a closed mold. The alloy samples were fabricated by arc melting of the pressed powders on a water-cooled copper crucible in an argon atmosphere. Then, the samples were annealed in vacuum at 800 °C for 10 h. The resulting ingots were cut into disks of 10 mm in diameter and 0.7 mm in thickness. Then, the samples were ground using SiC paper with a grain size up to 5 μm. Finally, the samples were annealed in vacuum at 800 °C for 6 h.

2.2. Characterization

The phase composition and crystalline structure of the fabricated alloys were analyzed by X-ray diffraction (XRD) using an XRD-7000S diffractometer (Shimadzu, Kyoto, Japan) with CuK_α radiation (1.5410 Å wavelength) at 40 kV and 30 mA in the Bragg-Brentano geometry. The phases were identified using the PDF4+ 2021 database and SIeve software (ICDD, Newtown, PA, USA). The phase composition and lattice parameters were calculated by Rietveld refinement. The microstructure and elemental composition of the samples were analyzed by scanning electron microscopy (SEM) using Vega 3 (Tescan, Brno, Czech Republic) equipped with an energy dispersive X-ray spectroscopy (EDX) attachment.

2.3. Hydrogen Permeation Tests

For the hydrogen permeation test, the samples were placed in the test cell with a copper seal gasket (Figure 1). The surface of the samples was covered by thin Pd film using magnetron sputtering. The active surface area of the membrane samples was 1.9×10^{-5} m². Leak testing was carried out before and after the experiment. Hydrogen was supplied from one side of the membrane at room temperature. From the side of the gas outlet, the

hydrogen signal was analyzed by a mass spectrometer. The experiment was started after the leakage test was valid. The chamber was evacuated to the residual pressure of 10^{-3} Pa from both sides of the sample. The sample was heated to 300–500 °C with a heating rate of 6 °C/min. After reaching the heating temperature, hydrogen gas (4 bar) was supplied to the one side of the sample.
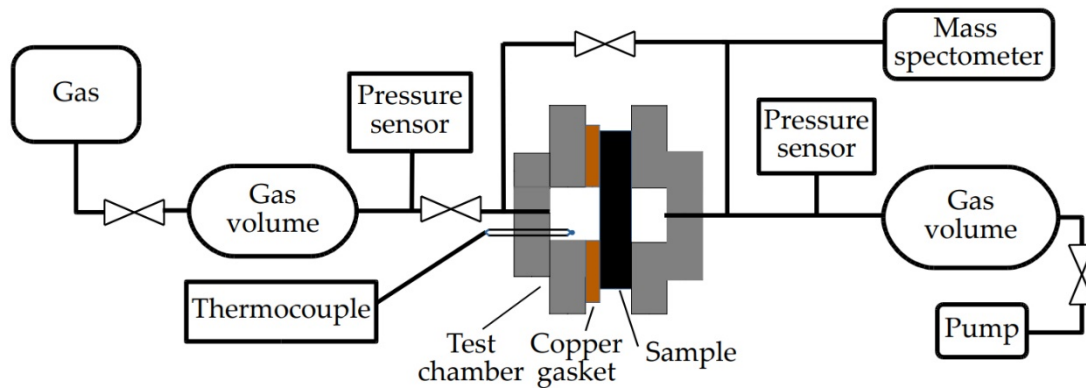

Figure 1. Schematic diagram of the test cell for hydrogen permeation experiments.

The concentration of hydrogen permeated through the sample was measured by the change in pressure in known volumes:

$$n(mol) = \frac{P \times V}{R \times T},$$
(1)

where P—pressure (Pa), V—volume (m^3), R—gas constant, T—temperature (K).

The flux (Φ) was calculated from the difference in the amount of gas passed through the area of the sample in a period of time:

$$\Phi = \frac{n1 - n2}{t \times S},$$
(2)

where $n1$—initial concentration of gas (mol), $n2$—final concentration of gas (mol), t—time (s), S—active surface area of the sample (m^2).

Hydrogen permeability was calculated according to the following expression [19]:

$$j = \Phi \times \frac{d}{\Delta P^{0.5}},$$
(3)

where d—sample thickness, ΔP—pressure difference.

2.4. Ab Initio Calculations

The binding energy for a hydrogen atom in Nb-Ni-Ti-Zr-Co high entropy alloys was theoretically investigated using first principles. All calculations were performed within the framework of the density functional theory using the optimized norm-preserving Vanderbilt pseudopotential [20], realized in the ABINIT software package [21,22] within virtual crystal approximation (VCA) [23,24]. To describe the exchange and correlation effects, the generalized gradient approximation in the form of Perdew, Burke, and Ernzerhof was used [25]. The lattices were completely relaxed. The relaxation was considered complete when the forces acting on the atoms were less than 25 meV/Å. To carry out the structural optimization and relaxation of the Nb-Ni-Ti-Zr-Co system for discussion, a cell with 2 atoms with mixing potentials and 1 H atom was adopted, and the k meshes were chosen to be $10 \times 10 \times 10$ for BCC structures. The cutoff energy for the plane-wave basis was set at 820 eV.

The binding energy of hydrogen atom in HEAs was calculated according to the following expression:

$$E_b = E(A_2) + \tfrac{1}{2}E(H_2) - E(A_2H), \tag{4}$$

where $E(A_2)$ is the energy of pure alloy in the presence of two mixing atoms in the cell; $E(H_2)$ is the energy of the hydrogen molecule; $E(A_2H)$ is the energy of the structure when there is a hydrogen atom in it.

3. Results

3.1. Microstructure and Phase Composition

The XRD patterns of $Nb_{20}Ni_{20}Ti_{20}Zr_{20}Co_{20}$ and $Nb_{40}Ni_{25}Ti_{18}Zr_{12}Co_5$ high entropy alloys after annealing at 800 °C for 10 h are presented in Figure 2. According to XRD measurements, equimolar $Nb_{20}Ni_{20}Ti_{20}Zr_{20}Co_{20}$ HEA consists of two BCC phases with lattice constants of 3.306 Å and 3.093 Å (Figure 2a). For non-equimolar $Nb_{40}Ni_{25}Ti_{18}Zr_{12}Co_5$ alloy, an Nb-rich BCC phase with the lattice constant of 3.306 Å and a B2-Ni(Ti, Zr) phase with the lattice constant of 3.060 Å were observed (Figure 2b). Additionally, weakly pronounced peaks of B2-CoZr compound were detected for the non-equimolar alloy.
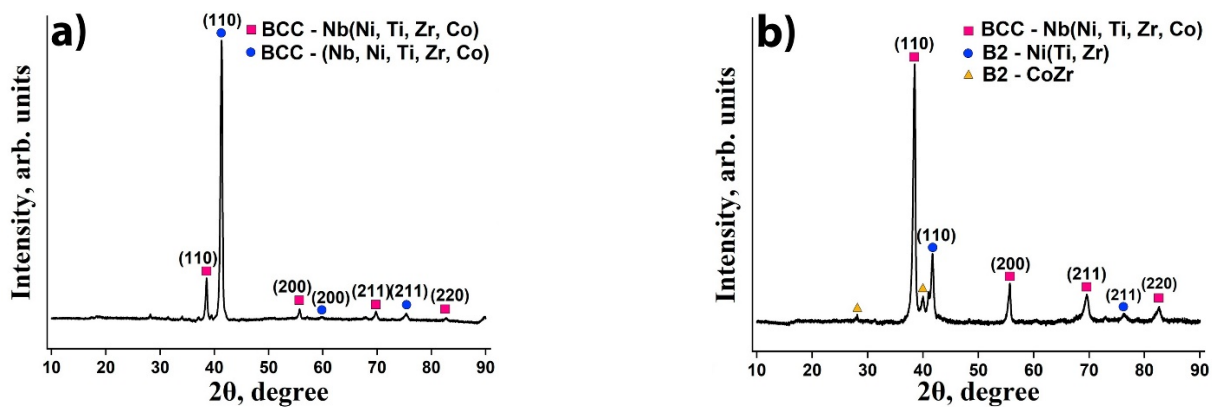

Figure 2. XRD patterns of $Nb_{20}Ni_{20}Ti_{20}Zr_{20}Co_{20}$ (**a**) and $Nb_{40}Ni_{25}Ti_{18}Zr_{12}Co_5$ (**b**) high entropy alloys annealed at 800 °C for 10 h.

Figure 3a shows the SEM image and corresponding EDS maps of the equimolar $Nb_{20}Ni_{20}Ti_{20}Zr_{20}Co_{20}$ alloy. Two major regions with different contrast can be seen: a light-grey contrasted Nb-rich BCC phase (region 1) with a globular and dendritic structure and a dark-grey contrasted—(Nb, Ni, Ti, Zr, Co) BCC phase (region 2), which has elemental content close to equimolar composition (Table 1).

Table 1. Elemental concentration in different regions as depicted in Figure 3.

Sample	Region	Concentration, at. %					Possible Phases
		Nb	Ni	Ti	Zr	Co	
$Nb_{20}Ni_{20}Ti_{20}Zr_{20}Co_{20}$	1	74	6	9	5	6	BCC-Nb(Ni, Ti, Zr, Co)
	2	15	20	16	29	19	BCC-(Nb, Ni, Ti, Zr, Co)
$Nb_{40}Ni_{25}Ti_{18}Zr_{12}Co_5$	3	88.8	3.7	6.5	-	0.9	BCC-Nb(Ni, Ti, Co)
	4	7.7	41.6	26.3	16.6	7.6	B2-Ni(Ti, Zr), B2-CoZr
	5	31	36	17.7	8.5	6.5	BCC-Nb(Ni, Ti, Zr, Co), B2-Ni(Ti, Zr)
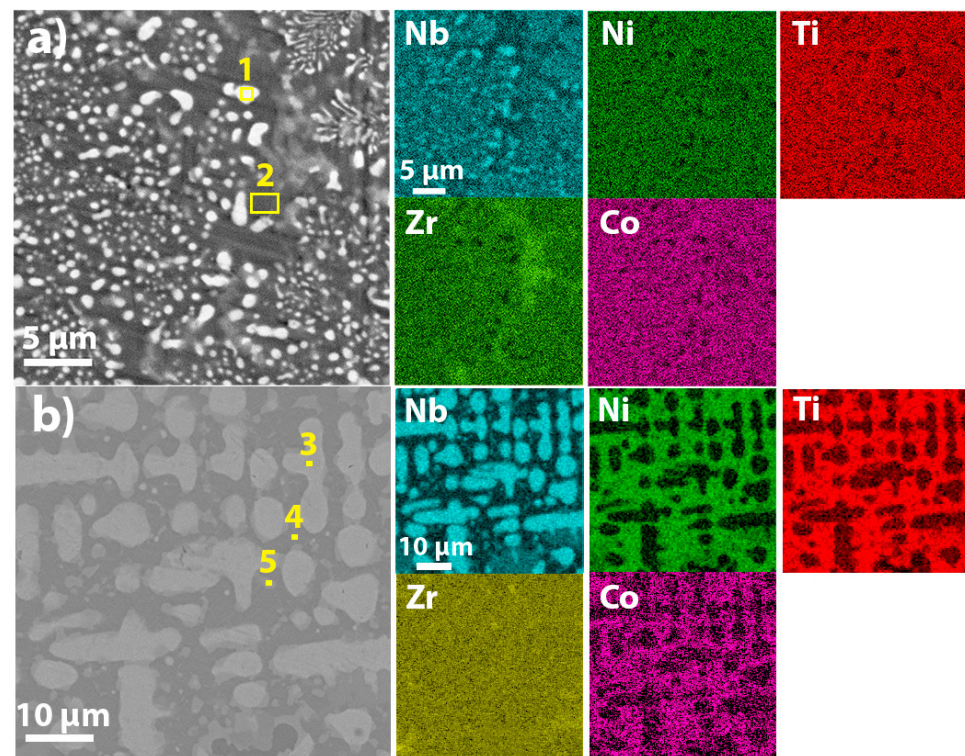
Figure 3. SEM images of $Nb_{20}Ni_{20}Ti_{20}Zr_{20}Co_{20}$ (**a**) and $Nb_{40}Ni_{25}Ti_{18}Zr_{12}Co_5$ (**b**) HEAs and corresponding EDS maps.

The microstructure of non-equimolar $Nb_{40}Ni_{25}Ti_{18}Zr_{12}Co_5$ (Figure 3b) high entropy alloy is represented by a light-grey contrasted Nb-rich BCC phase with dendritic structure (region 3) embedded in dark-grey contrasted matrix of B2-Ni(Ti, Zr) and B2-CoZr phases (region 4). Similar morphology and phases were observed by Tang et al. for $Nb_{40}Ti_{18}Zr_{12}Ni_{30}$ alloy [15]. Additionally, light-grey globular inclusions with high concentration of Nb (31 at.%) were detected in region 5. Since this also has high Ni content, it is assumed that this region corresponds to an Nb-enriched BCC-phase surrounded by a B2-Ni(Ti, Zr) phase.

3.2. Hydrogen Permeability

Figure 4 shows permeability curves for the HEA samples. The permeability of $Nb_{40}Ni_{25}Ti_{18}Zr_{12}Co_5$ obtained by Tang et al. was added to Figure 4 for comparison. To analyze the temperature effect, Arrhenius plots were constructed based on the data of linear approximation of the permeability rate on inverse temperature. The permeability of the equimolar alloy is higher at lower temperatures (300–350 °C), but lower at higher temperatures compared to the non-equimolar alloy. Approximation of the permeability by the Arrhenius equation for HEA alloys showed that the activation energy of permeability for $Nb_{20}Ni_{20}Ti_{20}Co_{20}Zr_{20}$ is 30 kJ/mol with pre-exponential factor 1.8×10^{-6}, and for $Nb_{40}Ni_{25}Ti_{18}Zr_{12}Co_5$ the activation energy is 38 kJ/mol with pre-exponential factor 1×10^{-5}. It can be seen that the activation energy of the equimolar high-entropy alloy is significantly lower than that for the non-equimolar $Nb_{40}Ti_{18}Zr_{12} Ni_{25}Co_5$ alloy. According to permeability tests, it was revealed that equimolar HEA is less susceptible to hydrogen embrittlement. The $Nb_{40}Ni_{25}Ti_{18}Zr_{12}Co_5$ alloy failed (crashed) after the 12 h permeation experiment. Under the same conditions, the equimolar HEA worked for more than 26 h without loss of performance.
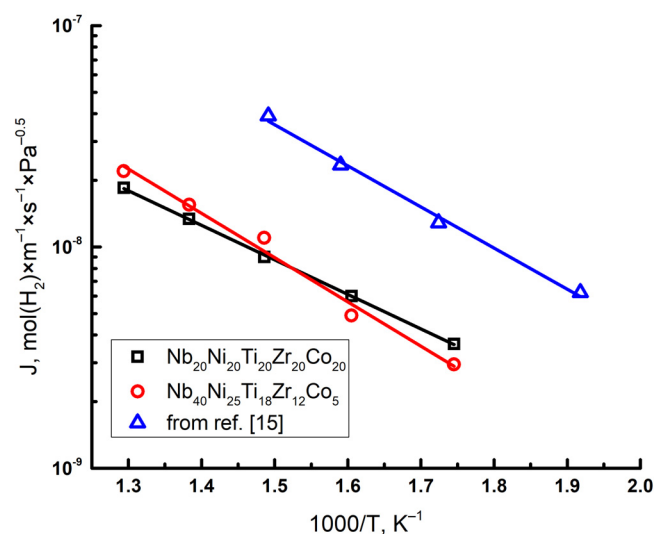
Figure 4. Hydrogen permeability of HEAs depending on temperature.

3.3. Lattice Constants and Hydrogen Binding Energy in HEAs

Table 2 summarizes the ab initio calculation results for lattice parameters and hydrogen binding energies in different phases of the HEAs. The overall dependence of the lattice constant changes depending on the elemental composition is in good correlation with the experimental results. The best agreement between the calculated results and experimental lattice parameters was observed for high niobium concentrations in the BCC lattice. However, in all cases the calculated lattice constant is underestimated, which can be caused by temperature effect, lattice strains in as-fabricated HEAs and features of the VCA.

Table 2. Lattice parameters and binding energies, *Eb*, for the hydrogen atom.

Alloy	Phase	Lattice Constant, Å				E_b, eV
		Exp	*a*, Calc	*b*, Calc	*c*, Calc	
$Nb_{74}Ni_6Ti_9Zr_5Co_6$	pure		3.192	3.192	3.192	-
	H in T sites	3.306	3.275	3.293	3.293	0.760
	H in O sites		3.137	3.137	3.586	0.441
$Nb_{15}Ni_{20}Ti_{16}Zr_{29}Co_{19}$	pure	3.090	2.979	2.979	2.979	-
	H in O sites		2.727	2.727	3.863	0.248
$Nb_{88.8}Ni_{3.7}Ti_{6.5}Co_{0.9}$	pure		3.251	3.251	3.251	-
	H in T sites	3.306	3.331	3.354	3.354	1.037
	H in O sites		3.196	3.196	3.641	0.777
$Nb_{7.7}Ni_{41.6}Ti_{26.32}Zr_{16.6}Co_{7.59}$	pure	3.060	2.855	2.855	2.855	-
	H in O sites		2.609	2.609	3.717	0.686

The difference in the changes in lattice parameters depending on the location of hydrogen atoms in BCC structure was found. The hydrogen atom in octahedral (O) sites leads to a lattice distortion along *c* axis at the octahedral coordination and all lattice expansion at the tetrahedral coordination in both BCC-Nb(Ni,Ti,Zr,Co) and BCC-(Nb,Ni,Ti,Zr,Co) phases.

The highest binding energy for hydrogen atoms was found at the high Nb concentration BCC lattice, which probably implies higher absorption of the hydrogen in regions with BCC-Nb(Ni,Ti,Zr,Co) phase. The decrease in Nb concentration leads to the decrease in the hydrogen binding energy in both T and O sites. In the $Nb_{15}Ni_{20}Ti_{16}Zr_{29}Co_{19}$ and $Nb_{7.7}Ni_{41.6}Ti_{26.32}Zr_{16.6}Co_{7.59}$ systems, the location of the hydrogen atom in tetrahedral sites

leads to system instability—a hydrogen atom leaves these sites. The lowest binding energy of the hydrogen atoms in the octahedral sites and the unstable tetrahedral configuration of hydrogen atoms can lead to the high hydrogen diffusivity in the BCC-(Nb,Ni,Ti,Zr,Co) lattice compared to Nb-rich BCC phase.

4. Discussion

The synthesized equimolar and non-equimolar HEAs have high hydrogen permeability, which depends on their microstructure and phase composition. The equimolar alloy has lower activation energy, and correspondingly higher permeability at lower temperatures (300–350 °C). This alloy is also more resistant to hydrogen embrittlement than the non-equimolar one containing a higher concentration of niobium. In the case of equimolar $Nb_{20}Ni_{20}Ti_{20}Zr_{20}Co_{20}$ HEA, a fine-dispersed structure with Nb-rich BCC-Nb(Ni,Ti,Zr,Co) and BCC-(Nb,Ni,Ti,Zr,Co) phases was obtained. Several studies have observed higher permeability of the multicomponent alloys with fine-dispersed structure, for example, for Nb–Ti–Co and Nb–Ni–Ti alloys [26–28]. Hashi et al. [26] and Yan et al. [27] also observed high resistance to hydrogen embrittlement for the fine grained alloy compared to coarse grained. Thus, the homogeneous fine microstructure of $Nb_{20}Ni_{20}Ti_{20}Zr_{20}Co_{20}$ HEA can have a positive effect both on the permeability of the alloy due to the large number of phase boundaries and on hydrogen embrittlement resistance. It is known that permeability depends on many factors, but the most important are solubility and diffusivity within the crystal lattice [29]. Niobium and its alloys are characterized by high hydrogen permeability due to high solubility limits and the relatively high diffusion mobility of hydrogen [30]. Based on ab initio calculations, hydrogen prefers to occupy tetrahedral sites in the Nb-based BCC lattice, which also agrees well with the results of other works [31]. The Nb-based crystal lattice also has a larger volume due to the larger lattice parameter of 3.306 A for the Nb-based BCC-Nb(Ni, Ti, Zr, Co) compared to the equimolar BCC-(Nb, Ni, Ti, Zr, Co) with the lattice parameter of 3.06 A. This provides higher solubility of the Nb-based BCC lattice in the HEAs. In turn, the low binding energy of hydrogen in the interstitial sites of the equimolar alloy can provide better diffusion mobility of hydrogen in the lattice but lower hydrogen absorption and hydrogen embrittlement. We believe that the competition between solubility and diffusivity can explain the observed difference in the permeability of HEAs. Based on the XRD data, the main phase in the equimolar alloy is BCC-(Nb, Ni, Ti, Zr, Co), while in the non-equimolar is BCC-Nb(Ni, Ti, Co). It should also be noted that the presence of secondary phases B2-Ni(Ti, Zr) and B2-CoZr in the $Nb_{40}Ni_{25}Ti_{18}Zr_{12}Co_5$ alloy can negatively affect its hydrogen permeability [26]. Thus, it is assumed that the high permeability of the $Nb_{40}Ni_{25}Ti_{18}Zr_{12}Co_5$ alloy at higher temperatures (400–500 °C) is provided mainly by the more permeable Nb-based BCC lattice with higher hydrogen solubility. While for the equimolar alloy, the high diffusivity of hydrogen through the BCC-(Nb, Ni, Ti, Zr, Co) along with the fine-dispersed structure provide lower activation energy and higher permeability at lower temperatures. In addition, it should be noted that the distortions of the crystal lattice in HEAs due to the difference in the atomic sizes in the structure make an additional contribution to the increase in hydrogen solubility. This can cause the difference in the behavior of permeability depending on the temperature for pure niobium and Nb-based multicomponent BCC structures.

5. Conclusions

High-entropy alloys with equimolar and non-equimolar compositions were synthesized by arc melting. Their microstructure, phase composition, hydrogen binding energy in interstitial sites as well as hydrogen permeability at 300–500 °C were studied. The following conclusions was made:

1. A fine-grained microstructure with BCC-(Nb, Ni, Ti, Zr, Co) and BCC-Nb(Ni, Ti, Zr, Co) lattices is formed in the equimolar $Nb_{20}Ni_{20}Ti_{20}Zr_{20}Co_{20}$ alloy, while coarser dendritic microstructure with Nb-enriched BCC-Nb(Ni, Ti, Co), B2-Ni(Ti, Zr) and B2-CoZr phases is presented in the $Nb_{40}Ni_{25}Ti_{18}Zr_{12}Co_5$ alloy.

2. The lattice parameter and hydrogen binding energy in the interstitial sites are higher for the Nb-enriched BCC lattice than that for the BCC lattice with near equimolar composition, which indicates higher hydrogen solubility in the Nb-enriched phase. The hydrogen binding energy decreases in both tetrahedral and octahedral sites in the BCC-(Nb, Ni, Ti, Zr, Co) lattice, which apparently causes higher diffusivity of hydrogen.

3. The $Nb_{20}Ni_{20}Ti_{20}Zr_{20}Co_{20}$ alloy shows lower activation energy and higher permeability at temperatures of 300–350 °C as well as higher resistance to hydrogen embrittlement.

The obtained results give prospects for the development of HEA-based metallic membranes for hydrogen separation and purification.

References

1. Ockwig, N.W.; Nenoff, T.M. Membranes for Hydrogen Separation. *Chem. Rev.* **2007**, *107*, 4078–4110. [CrossRef]
2. Dolan, M.D. Non-Pd BCC Alloy Membranes for Industrial Hydrogen Separation. *J. Membr. Sci.* **2010**, *362*, 12–28. [CrossRef]
3. Conde, J.J.; Maroño, M.; Sánchez-Hervás, J.M. Pd-Based Membranes for Hydrogen Separation: Review of Alloying Elements and Their Influence on Membrane Properties. *Sep. Purif. Rev.* **2017**, *46*, 152–177. [CrossRef]
4. Lu, G.Q.; Diniz da Costa, J.C.; Duke, M.; Giessler, S.; Socolow, R.; Williams, R.H.; Kreutz, T. Inorganic Membranes for Hydrogen Production and Purification: A Critical Review and Perspective. *J. Colloid Interface Sci.* **2007**, *314*, 589–603. [CrossRef] [PubMed]
5. Li, F.; Zhong, B.; Xiao, H.; Ye, X.; Lu, L.; Guan, W.; Zhang, Y.; Wang, X.; Chen, C. Effect of Degassing Treatment on the Deuterium Permeability of Pd-Nb-Pd Composite Membranes during Deuterium Permeation. *Sep. Purif. Technol.* **2018**, *190*, 136–142. [CrossRef]
6. Phair, J.W.; Donelson, R. Developments and Design of Novel (Non-Palladium-Based) Metal Membranes for Hydrogen Separation. *Ind. Eng. Chem. Res.* **2006**, *45*, 5657–5674. [CrossRef]
7. Yan, E.; Min, R.N.; Zhao, P.; Misra, R.D.K.; Huang, P.R.; Zou, Y.J.; Chu, H.L.; Zhang, H.Z.; Xu, F.; Sun, L.X. Design of Nb-Based Multi-Phase Alloy Membranes for High Hydrogen Permeability and Suppressed Hydrogen Embrittlement. *J. Membr. Sci.* **2020**, *595*, 117531. [CrossRef]
8. Nambu, T.; Shimizu, K.; Matsumoto, Y.; Rong, R.; Watanabe, N.; Yukawa, H.; Morinaga, M.; Yasuda, I. Enhanced Hydrogen Embrittlement of Pd-Coated Niobium Metal Membrane Detected by in Situ Small Punch Test under Hydrogen Permeation. *J. Alloys Compd.* **2007**, *446–447*, 588–592. [CrossRef]
9. Magnone, E.; Jeon, S.I.; Park, J.H.; Fleury, E. Relationship between Microstructure and Hydrogen Permeation Properties in the Multiphase Ni21Ti23Nb56 Alloy Membranes. *J. Membr. Sci.* **2011**, *384*, 136–141. [CrossRef]
10. Wang, N.J.; Liu, Y. Microstructure of Nb-Ta-V Based Hydrogen Permeation High Entropy Alloys. *Mater. Sci. Forum* **2016**, *849*, 3–7. [CrossRef]
11. Kishida, K.; Yamaguchi, Y.; Tanaka, K.; Inui, H.; Tokui, S.; Ishikawa, K.; Aoki, K. Microstructures and Hydrogen Permeability of Directionally Solidified Nb–Ni–Ti Alloys with the Nb–NiTi Eutectic Microstructure. *Intermetallics* **2008**, *16*, 88–95. [CrossRef]
12. Jiang, P.; Huang, H.; Sun, B.; Song, G.; Wu, W.; Wang, Z.; Zhang, Y. Microstructure, Mechanical Properties and Hydrogen Permeability of Multiphase V-Ti-Ni Alloy Membranes. *Mater. Today Commun.* **2020**, *24*, 101112. [CrossRef]
13. Belyakova, R.M.; Kurbanova, E.D.; Sidorov, N.I.; Polukhin, V.A. Nb–Ni- and V–Ni-Based Membranes for High-Purity Hydrogen Production. *Russ. Metall. Met.* **2022**, *2022*, 851–860. [CrossRef]
14. Shimpo, Y.; Yamaura, S.-I.; Nishida, M.; Kimura, H.; Inoue, A. Development of Melt-Spun Ni–Nb–Zr–Co Amorphous Alloy for High-Performance Hydrogen Separating Membrane. *J. Membr. Sci.* **2006**, *286*, 170–173. [CrossRef]
15. Tang, H.X.; Ishikawa, K.; Aoki, K. Effect of Elements Addition on Hydrogen Permeability and Ductility of Nb40Ti18Zr12Ni30 Alloy. *J. Alloys Compd.* **2008**, *461*, 263–266. [CrossRef]
16. Divinski, S.V.; Lukianova, O.A.; Wilde, G.; Dash, A.; Esakkiraja, N.; Paul, A. High-Entropy Alloys: Diffusion. In *Encyclopedia of Materials: Metals and Alloys*; Caballero, F.G., Ed.; Elsevier: Oxford, UK, 2022; pp. 402–416. ISBN 978-0-12-819733-2.

17. Cheng, C.-Y.; Yang, Y.-C.; Zhong, Y.-Z.; Chen, Y.-Y.; Hsu, T.; Yeh, J.-W. Physical Metallurgy of Concentrated Solid Solutions from Low-Entropy to High-Entropy Alloys. *Curr. Opin. Solid State Mater. Sci.* **2017**, *21*, 299–311. [CrossRef]
18. Han, Z.; Liu, X.; Zhao, S.; Shao, Y.; Li, J.; Yao, K. Microstructure, Phase Stability and Mechanical Properties of Nb–Ni–Ti–Co–Zr and Nb–Ni–Ti–Co–Zr–Hf High Entropy Alloys. *Prog. Nat. Sci. Mater. Int.* **2015**, *25*, 365–369. [CrossRef]
19. Suzuki, A.; Yukawa, H. A Review for Consistent Analysis of Hydrogen Permeability through Dense Metallic Membranes. *Membranes* **2020**, *10*, 120. [CrossRef] [PubMed]
20. Hamann, D.R. Optimized Norm-Conserving Vanderbilt Pseudopotentials. *Phys. Rev. B* **2013**, *88*, 085117. [CrossRef]
21. Gonze, X.; Amadon, B.; Antonius, G.; Arnardi, F.; Baguet, L.; Beuken, J.-M.; Bieder, J.; Bottin, F.; Bouchet, J.; Bousquet, E. The ABINIT Project: Impact, Environment and Recent Developments. *Comput. Phys. Commun.* **2020**, *248*, 107042. [CrossRef]
22. Romero, A.H.; Allan, D.C.; Amadon, B.; Antonius, G.; Applencourt, T.; Baguet, L.; Bieder, J.; Bottin, F.; Bouchet, J.; Bousquet, E. ABINIT: Overview and Focus on Selected Capabilities. *J. Chem. Phys.* **2020**, *152*, 124102. [CrossRef]
23. Bellaiche, L.; Vanderbilt, D. The Virtual Crystal Approximation Revisited: Application to Dielectric and Piezoelectric Properties of Perovskites. *Phys. Rev. B* **2000**, *61*, 7877–7882. [CrossRef]
24. Ghosez, P.; Desquesnes, D.; Gonze, X.; Rabe, K.M. First-Principles Study of Lattice Instabilities in $Ba_xSr_{1-x}TiO_3$. *AIP Conference Proceedings* **2000**, *535*, 102–110.
25. Perdew, J.P.; Burke, K.; Ernzerhof, M. Generalized Gradient Approximation Made Simple. *Phys. Rev. Lett.* **1996**, *77*, 3865–3868. [CrossRef]
26. Hashi, K.; Ishikawa, K.; Matsuda, T.; Aoki, K. Microstructure and Hydrogen Permeability in Nb–Ti–Co Multiphase Alloys. *J. Alloys Compd.* **2006**, *425*, 284–290. [CrossRef]
27. Yan, E.; Li, X.; Rettenmayr, M.; Liu, D.; Su, Y.; Guo, J.; Xu, D.; Fu, H. Design of Hydrogen Permeable Nb–Ni–Ti Alloys by Correlating the Microstructures, Solidification Paths and Hydrogen Permeability. *Int. J. Hydrog. Energy* **2014**, *39*, 3505–3516. [CrossRef]
28. Ishikawa, K.; Tokui, S.; Aoki, K. Microstructure and Hydrogen Permeation of Cold Rolled and Annealed Nb40Ti30Ni30 Alloy. *Intermetallics* **2009**, *17*, 109–114. [CrossRef]
29. Santucci, A.; Tosti, S.; Basile, A. 4—Alternatives to Palladium in Membranes for Hydrogen Separation: Nickel, Niobium and Vanadium Alloys, Ceramic Supports for Metal Alloys and Porous Glass Membranes. In *Handbook of Membrane Reactors*; Basile, A., Ed.; Woodhead Publishing: Sawston, Cambridge, UK, 2013; Volume 1, pp. 183–217. ISBN 978-0-85709-414-8.
30. Yukawa, H.; Nambu, T.; Matsumoto, Y.; Watanabe, N.; Zhang, G.; Morinaga, M. Alloy Design of Nb-Based Hydrogen Permeable Membrane with Strong Resistance to Hydrogen Embrittlement. *Mater. Trans.* **2008**, *49*, 2202–2207. [CrossRef]
31. Ramachandran, A.; Zhuang, H.; Lackner, K.S. Probing the Interactions between Interstitial Hydrogen Atoms in Niobium through Density Functional Theory Calculations. *Mater. Today Commun.* **2020**, *25*, 101415. [CrossRef]